THE JOURNAL OF BIOLOGICAL CHEMISTRY VOL. 283, NO. 51, pp. 35703–35714, December 19, 2008

Critical Interaction of Actuator Domain Residues Arginine 174, Isoleucine 188, and Lysine 205 with Modulatory Nucleotide in Sarcoplasmic Reticulum Ca^{2+}-ATPase*[S]

Received for publication, September 2, 2008, and in revised form, September 29, 2008 Published, JBC Papers in Press, October 17, 2008, DOI 10.1074/jbc.M806795200

Johannes D. Clausen[‡§], David B. McIntosh[¶], David G. Woolley[¶], and Jens Peter Andersen[‡§1]

From the [‡]Department of Physiology and Biophysics, Aarhus University, DK-8000 Aarhus C, Denmark, the [¶]Institute of Infectious Diseases and Molecular Medicine, Division of Chemical Pathology, Faculty of Health Sciences, University of Cape Town, Observatory, Cape Town 7925, South Africa, and the [§]Centre for Membrane Pumps in Cells and Disease-PUMPKIN, Danish National Research Foundation, Denmark

ATP plays dual roles in the reaction cycle of the sarcoplasmic reticulum Ca^{2+}-ATPase by acting as the phosphorylating substrate as well as in nonphosphorylating (modulatory) modes accelerating conformational transitions of the enzyme cycle. Here we have examined the involvement of actuator domain residues Arg^{174}, Ile^{188}, Lys^{204}, and Lys^{205} by mutagenesis. Alanine mutations to these residues had little effect on the interaction of the Ca_2E1 state with nucleotide or on the H_nE2 to Ca_2E1 transition of the dephosphoenzyme. The phosphoenzyme processing steps, Ca_2E1P to $E2P$ and $E2P$ dephosphorylation, and their stimulation by MgATP/ATP were markedly affected by mutations to Arg^{174}, Ile^{188}, and Lys^{205}. Replacement of Ile^{188} with alanine abolished nucleotide modulation of dephosphorylation but not the modulation of the Ca_2E1P to $E2P$ transition. Mutation to Arg^{174} interfered with nucleotide modulation of either of the phosphoenzyme processing steps, indicating a significant overlap between the modulatory nucleotide-binding sites involved. Mutation to Lys^{205} enhanced the rates of the phosphoenzyme processing steps in the absence of nucleotide and disrupted the nucleotide modulation of the Ca_2E1P to $E2P$ transition. Remarkably, the mutants with alterations to Lys^{205} showed an anomalous inhibition by ATP of the dephosphorylation, and in the alanine mutant the affinity for the inhibition by ATP was indistinguishable from that for stimulation by ATP of the wild type. Hence, the actuator domain is an important player in the function of ATP as modulator of phosphoenzyme processing, with Arg^{174}, Ile^{188}, and Lys^{205} all being critically involved, although in different ways. The data support a variable site model for the modulatory effects with the nucleotide binding somewhat differently in each of the conformational states occurring during the transport cycle.

The sarcoplasmic reticulum Ca^{2+}-ATPase (1) is a membrane-bound ion pump that belongs to the family of P-type ATPases (2), named so because their reaction cycles involve the transient phosphorylation of the aspartic acid residue in the universally conserved DKTGT(L/I)T motif. Insight into the structural organization and domain movements that take place during pump activity in P-type ATPases has come from the elucidation over the past 8 years of several high resolution crystal structures of Ca^{2+}-ATPase (3–11), each thought to represent a specific intermediate state in the pump cycle (12), as well as the recent crystal structures of pig renal Na^+,K^+-ATPase (13) and *Arabidopsis thaliana* H^+-ATPase (14). In these P-type pumps the membrane-buried region is made up of 10 membrane-spanning α-helices. The cytoplasmic headpiece is separated into three distinct domains, named A ("actuator"), P ("phosphorylation"), and N ("nucleotide binding"). The ion translocation is achieved by sequential conformational transitions between phosphorylated and dephosphorylated intermediate states (*cf.* Scheme 1 for Ca^{2+}-ATPase) (15, 16). The key to understanding the long distance coupling between formation/decomposition of the acyl phosphate in the cytoplasmic P-domain and the changes in the ion-binding sites buried deep in the membranous region seems to be the relatively large movements of the A-domain, which are transmitted to the transmembrane helices (8, 11).

ATP plays dual roles in the reaction cycle of the Ca^{2+}-ATPase by acting both as the phosphorylating substrate as well as in nonphosphorylating (modulatory) modes, the latter regulating the rates of various partial reaction steps (*boxed ATP* in Scheme 1). The modulatory action of ATP seems to be a general feature in the family of P-type pumps and is a vital means of overcoming rate-limiting reaction steps during pump activity. Thus, the K^+ deoccluding $K_nE2 \rightarrow E1$ transition in Na^+,K^+-ATPase and H^+,K^+-ATPase as well as the corresponding $H_nE2 \rightarrow E1$ transition in Ca^{2+}-ATPase are accelerated by ATP with affinity constants in the 10–100 μM range (17–21). In the Ca^{2+}-ATPase, ATP furthermore binds to the phosphoenzyme intermediates and stimulates phosphoenzyme turnover (*i.e.* $Ca_2E1P \rightarrow E2P$ and $E2P \rightarrow E2$ partial reactions (22–30)), whereas in Na^+,K^+-ATPase the rate of $E2P$ dephosphorylation seems instead to be inhibited by nucleotide (31, 32). Such observations have raised the question whether the modulatory ATP molecule binds at the same site as the ATP molecule undergo-

* This work was supported in part by grants from the Danish Medical Research Council, the Danish National Research Foundation (PUMPKIN Centre), the Novo Nordisk Foundation, Denmark, the Lundbeck Foundation, Denmark, the Research Foundation of Aarhus University (to J. P. A.), and the National Research Foundation of South Africa (to D. B. M.). The costs of publication of this article were defrayed in part by the payment of page charges. This article must therefore be hereby marked "*advertisement*" in accordance with 18 U.S.C. Section 1734 solely to indicate this fact.

[S] The on-line version of this article (available at http://www.jbc.org) contains supplemental Figs. S1–S8 and additional references.

[1] To whom correspondence should be addressed: Dept. of Physiology and Biophysics, Aarhus University, Ole Worms Allé 1185, DK-8000 Aarhus C, Denmark. Fax: 45-86129065; E-mail: jpa@fi.au.dk.

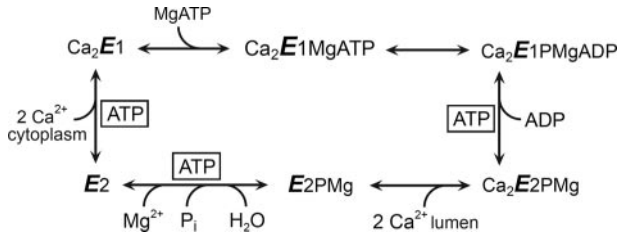

SCHEME 1. **Ca^{2+}-ATPase reaction cycle.** Major conformational changes and ligand binding and dissociation steps are shown. *Boxed ATP* indicates steps for which the rate is enhanced by additional binding of ATP or MgATP that is not hydrolyzed ("modulatory ATP").

ing hydrolysis (28, 33, 34) or at a distinct or only partially overlapping site (35, 36). In a recent mutagenesis study (30), we pinpointed Glu^{439}, Phe^{487}, and Arg^{560} in the N-domain and Arg^{678} in the P-domain of Ca^{2+}-ATPase as critical amino acid residues for the stimulation by ATP of *E*2P dephosphorylation. Phe^{487}, Arg^{560}, and Arg^{678} are also known as key residues in ATP binding in the phosphorylating mode (5, 7, 30, 37). None of these residues, however, were critical for the modulation by nucleotide of the $Ca_2E1P \rightarrow E2P$ transition, suggesting that yet undefined additional residues might be important in this case, but Arg^{678} proved essential also for the acceleration by MgATP of the $H_nE2 \rightarrow Ca_2E1$ transition. Because the A-domain plays a central role in the energy transduction and is closely associated with the catalytic site in *E*2 forms (38), it is relevant to ask whether A-domain residues might be involved in the modulatory effect of ATP, at least in *E*2 forms. Here we extend the previous analysis to include Arg^{174}, Ile^{188}, Lys^{204}, and Lys^{205} in the A-domain, and we demonstrate, for the first time, that the A-domain is a critical contributor to the binding and actions of modulatory nucleotide in Ca^{2+}-ATPase.

EXPERIMENTAL PROCEDURES

Site-directed mutagenesis of cDNA encoding the rabbit fast twitch muscle Ca^{2+}-ATPase (SERCA1a isoform) inserted into the pMT2 vector (39) was carried out using the QuikChange site-directed mutagenesis kit (Stratagene), and the mutant cDNA was sequenced throughout. To express wild type or mutant cDNA, COS-1 cells were transfected using the calcium phosphate precipitation method. Microsomal vesicles containing either expressed wild type or mutant Ca^{2+}-ATPase were isolated by differential centrifugation (40). The concentration of expressed Ca^{2+}-ATPase was determined by an enzyme-linked immunosorbent assay (41). Transport of $^{45}Ca^{2+}$ into the microsomal vesicles was measured by filtration, and the ATPase activity was determined by following the liberation of P_i in the presence of 4 μM ionophore A23187 to prevent inhibition caused by rebinding of Ca^{2+} to the lumenally facing Ca^{2+} sites (42, 43). Measurements of phosphorylation and dephosphorylation at 0 °C were carried out by manual mixing (30, 43, 44). Transient state kinetics at 25 °C was analyzed using the Bio-Logic quench-flow module QFM-5 (Bio-Logic Science Instruments, Claix, France) with mixing protocols as described previously (45). The determination of the phosphorylation level by acid quenching followed by acid SDS-PAGE and quantification of the radioactivity associated with the Ca^{2+}-ATPase band, as well as the photolabeling with [γ-^{32}P]TNP-8N_3-ATP,[2] the inhibition of photolabeling by ATP, and the quantification of the label bound specifically to the Ca^{2+}-ATPase were carried out using the previously established procedures (30, 37, 46–50).

The experiments were generally conducted at least twice, and average values are shown in the figures. The data were analyzed by nonlinear regression using the SigmaPlot program (SPSS, Inc.) or by computation using the SimZyme program (45). Monoexponential functions were fitted to the dephosphorylation time courses. The data obtained in rapid kinetic experiments using quench flow instrumentation were analyzed by the SimZyme program using a three-intermediate reaction scheme, taking into account the contribution by forward phosphoenzyme- and dephosphoenzyme-processing steps to the time course of phosphoenzyme formation, as detailed below and in previous publications (45, 51). The analysis of Ca^{2+} and MgATP concentration dependences of phosphorylation was based on the Hill equation, $EP = EP_{max} \cdot [L]^n/(K_{0.5}{}^n + [L]^n)$. A hyperbolic function plus a linear component was fitted to the [γ-^{32}P]TNP-8N_3-ATP labeling data, and the "true" dissociation constant, K_D, for ATP binding was calculated from the measured $K_{0.5}$ values using the validated equation for competitive inhibition (46). For analysis of the modulatory effect of nucleotide or PP_i (abbreviated "S" for substrate) on the rates of the partial reaction steps, the substrate concentration dependence of the rate constant was analyzed according to Equation 1,

$$k_{obs} = k_0 + (k_{max} - k_0)[S]/(K_{0.5} + [S]) \qquad \text{(Eq. 1)}$$

Here, k_{obs} is the rate constant observed at the indicated substrate concentration; k_0 is the rate constant in the absence of substrate ("basic rate"), and k_{max} is the extrapolated value of the rate constant corresponding to infinite substrate concentration. The enhancement factor k_{max}/k_0 describes the extent of the modulatory effect, and the $K_{0.5}$ value describes the affinity for the modulatory substrate.

RESULTS

Expression and Assays of Overall Function—Eight single mutations were introduced to four amino acid residues in the A-domain of sarcoplasmic reticulum Ca^{2+}-ATPase. Arg^{174}, Lys^{204}, and Lys^{205} were each substituted with alanine and glutamate, to examine the consequences of either removing the bulky, charged side chain or reversing the charge, and Ile^{188} was replaced by alanine and phenylalanine, to examine the importance of the size of the hydrophobic side chain at position 188. The expression levels in COS-1 cells of the six mutant pumps with alterations to Arg^{174}, Ile^{188}, and Lys^{205} were similar to that obtained with wild type, as evaluated by their immunoreactivity in the specific enzyme-linked immunosorbent assay (data not shown). The expression levels of mutants K204A and K204E were generally around 60 and 10–20%, respectively, of that

[2] The abbreviations used are: TNP-8N_3-ATP, 2′,3′-*O*-(2,4,6-trinitrophenyl)-8-azidoadenosine 5′-triphosphate; AMPPCP, adenosine 5′-(β,γ-methylene)-triphosphate; AMPPNP, adenosine 5′-(β,γ-imido)-triphosphate; EPPS, *N*-2-hydroxyethylpiperazine-*N*′-3-propanesulfonic acid; MES, 2-(*N*-morpholino)ethanesulfonic acid; MOPS, 3-(*N*-morpholino)propanesulfonic acid; PP_i, pyrophosphate; SERCA, sarco/endoplasmic reticulum Ca^{2+}-ATPase.

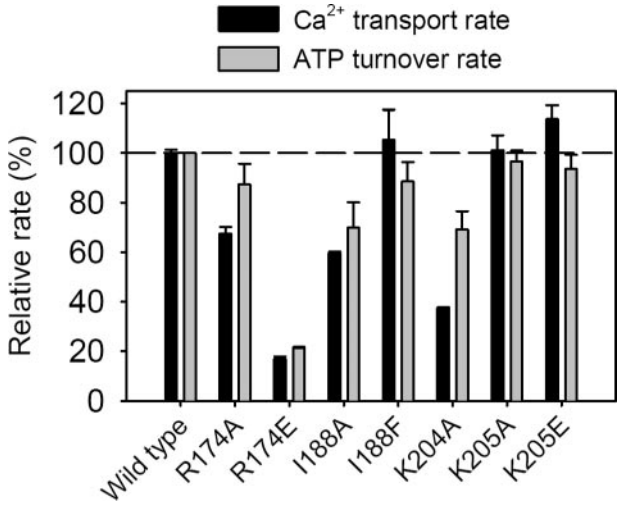

FIGURE 1. **Rates of ATP-driven Ca^{2+} transport and ATPase activity at 37 °C.** Measurements of ATP-driven Ca^{2+} transport (*black bars*) were performed by filtration following incubation for 5 min at 37 °C in 20 mM MOPS/Tris (pH 6.8), 100 mM KCl, 5 mM MgATP, 5 mM potassium oxalate (included to trap Ca^{2+} inside the microsomal vesicles), 0.5 mM EGTA, and 0.45 mM $^{45}CaCl_2$. The Ca^{2+} transport activity of the wild type was taken as 100%, and each mutant was related to this level following subtraction of the background activity determined with microsomes harvested from mock-transfected COS-1 cells and correction for the variation in expression level. The rate of Ca^{2+}-activated ATP hydrolysis (*gray bars*) was determined at 37 °C in 50 mM MOPS/Tris (pH 7.0), 100 mM KCl, 7 mM $MgCl_2$, 1 mM EGTA, 0.9 mM $CaCl_2$ (giving a free Ca^{2+} concentration of 3 μM), 4 μM Ca^{2+} ionophore A23187, and 5 mM ATP. The activity was calculated as the amount of P_i liberated per s, following subtraction of the background activity determined in the absence of Ca^{2+} and correction for the variation in expression level.

obtained with wild type. Reliable and reproducible biochemical experiments could be performed with K204A, whereas the low expression level of K204E precluded a functional characterization of this mutant.

For R174A, I188F, K205A, and K205E, the molecular rate of Ca^{2+}-activated ATP hydrolysis ("ATP turnover rate") at 37 °C with 5 mM MgATP was similar to, or slightly lower than (by less than 15%), that of wild type (Fig. 1). I188A and K204A displayed ~30% reduced ATP turnover rates relative to wild type, whereas the ATP turnover rate of R174E was reduced by as much as ~80%. The effects of the mutations to Arg^{174} on overall ATP turnover are similar to those presented previously (52). The overall activity at 37 °C and saturating substrate concentrations was further evaluated by measuring the ATP-driven accumulation of $^{45}Ca^{2+}$ in the microsomal vesicles (Fig. 1). For the mutants with alterations to Arg^{174}, Ile^{188}, and Lys^{205}, the rates of Ca^{2+} transport and ATP hydrolysis correlated well, implying that the coupling between ATP consumption and Ca^{2+} translocation is fully retained in the mutants. Mutant K204A, however, displayed only ~40% Ca^{2+} transport relative to wild type, compared with its ~70% rate of ATP turnover.

The Ca^{2+} dependence of the steady-state phosphoenzyme level obtained by phosphorylation from 5 μM [γ-^{32}P]MgATP and the [γ-^{32}P]MgATP dependence of steady-state phosphorylation at 100 μM free Ca^{2+} were determined at 0 °C and pH 7 (supplemental Fig. S1, *left* and *right panels*, respectively). At 10–100 μM free Ca^{2+} and 5–50 μM MgATP, the concentration ranges of Ca^{2+} and MgATP applied in the phosphorylation experiments described below, both the wild type and the mutants displayed high levels of phosphoenzyme (>80% of the EP_{max} derived from the fits of the Hill equation to the data).

Transient State Kinetics of Phosphorylation of Ca_2E1 from MgATP—The time course of phosphorylation from 10 μM [γ-^{32}P]MgATP of wild type or mutant Ca^{2+}-ATPase pre-equilibrated with Ca^{2+} was studied at pH 6 and 25 °C using rapid kinetics instrumentation (Fig. 2 and Table 1). Under these conditions, the wild type displays an initial overshoot of phosphorylation because of the contribution to rate limitation by the Ca^{2+} binding transition (*i.e.* $H_nE2 \rightarrow Ca_2E1$), causing a significant amount of dephosphoenzyme to accumulate at steady state. This overshoot can be reproduced by computer simulation based on the simplified three-intermediate reaction cycle shown in the *bottom right corner* of Fig. 2, with rate constants $k_A = 65\ s^{-1}$ for phosphorylation of Ca_2E1, $k_B = 3\ s^{-1}$ for phosphoenzyme processing (*i.e.* $Ca_2E1P \rightarrow E2P \rightarrow E2$, the latter step

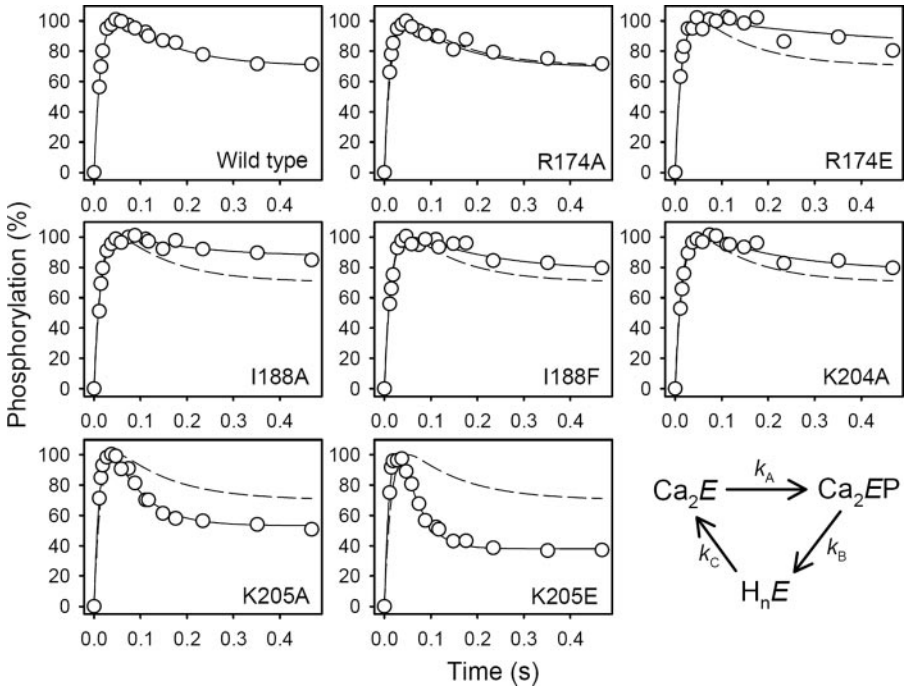

FIGURE 2. **Transient kinetics of phosphorylation of Ca_2E_1 with [γ-^{32}P]ATP.** Using a QFM-5 quench-flow module at 25 °C, microsomes suspended in 40 mM MES/Tris (pH 6.0), 80 mM KCl, 5 mM $MgCl_2$, and 100 μM $CaCl_2$ were mixed with an equal amount of the same medium containing [γ-^{32}P]ATP to produce a final concentration of 10 μM, followed by acid quenching at the indicated time intervals. The *lines* show the best fits to the data obtained by computation based on the reaction scheme shown in the *bottom right corner* using the SimZyme program (45), giving the rate constants for $Ca_2E_1 \rightarrow Ca_2E_1P$ (k_A) listed in Table 1. In each case, the maximum phosphorylation level was taken as 100%. The *broken lines* correspond to the wild type curve from the *top left panel*.

TABLE 1
Rate constants for partial reactions in the absence of excess (modulating) nucleotide

	$Ca_2E1 \rightarrow Ca_2E1P$[a]	$Ca_2E1P \rightarrow E2P$[b]	$E2P \rightarrow E2$[c]	$H_nE2 \rightarrow Ca_2E1$[d]
	s^{-1}	s^{-1}	min^{-1}	s^{-1}
Wild type	65	0.12	2.0	1.0
R174A	80	0.08	3.6	1.9
R174E	80	0.015	8.2	2.7
I188A	70	0.044	1.3	1.2
I188F	70	0.12	1.2	1.0
K204A	65	0.12	1.9	0.55
K205A	75	0.23	7.2	1.3
K205E	65	0.47	15.7	0.8

[a] Rate of phosphorylation from 10 μM [γ-^{32}P]MgATP of Ca^{2+}-saturated enzyme at 25 °C and at pH 6 derived from the computer simulation analysis of the data presented in Fig. 2 (detailed in the figure legends).
[b] Rate of forward processing of Ca_2E1P measured at pH 7 and 0 °C in the absence of excess (modulating) nucleotide (detailed in the legend to supplemental Fig. S4).
[c] Rate of $E2P$ dephosphorylation measured at pH 7 and 0 °C in the absence of nucleotide (detailed in the legend to supplemental Fig. S5).
[d] Rate of $H_nE2 \rightarrow Ca_2E1$ measured at pH 6 and 25 °C in the absence of nucleotide (detailed in the legend to supplemental Fig. S7*A*).

being much faster than the former under the conditions applied here, thus allowing them to be represented by a single rate constant), and $k_C = 5\ s^{-1}$ for the $H_nE2 \rightarrow Ca_2E1$ reaction sequence. With these rate constants the steady state is reached within ~0.5 s in the wild type, and after this point 36% of the enzyme is in the $E2$ state, 3% in the Ca_2E1 state, and 61% is phosphorylated.

As seen in Fig. 2 and Table 1, all seven mutants displayed phosphorylation rates in the 65–80 s^{-1} range (column labeled "$Ca_2E1 \rightarrow Ca_2E1P$" in Table 1), *i.e.* at least as fast as that of wild type, implying that Arg^{174}, Ile^{188}, Lys^{204}, and Lys^{205} are not critical for the transfer of the γ-phosphate from MgATP to Asp^{351} in the Ca_2E1 form. Because the phosphorylation was carried out at a subsaturating concentration of MgATP (the K_D for MgATP at pH 6 and 20 °C is ~10 μM (53, 54)), the wild type-like phosphorylation rates of the mutants furthermore suggest that Arg^{174}, Ile^{188}, Lys^{204}, and Lys^{205} are not critical for binding of MgATP to Ca^{2+}-saturated $E1$, as any change in nucleotide affinity induced by the mutations should also affect the phosphorylation rate (see below for direct measurements of MgATP binding to Ca^{2+}-free $E1$).

K205A and K205E both displayed more pronounced phosphorylation overshoots relative to wild type, with substantial levels of dephosphoenzyme accumulated at steady state (Fig. 2), implying either rapid phosphoenzyme processing or inhibition of the Ca^{2+} binding transition of the dephosphoenzyme. In such cases where the phosphorylation overshoot is substantial, fairly accurate values of k_B and k_C can be derived from the computer simulations, because the steepness of the descending phase following the overshoot directly reflects the rate of phosphoenzyme processing (51). The computational analysis showed that phosphoenzyme processing was 2.7- and 6-fold enhanced for K205A and K205E, respectively, relative to wild type, whereas the Ca^{2+} binding $H_nE2 \rightarrow Ca_2E1$ transition was rather unaffected by the mutations. For the remaining mutants, the size of the phosphorylation overshoot was either similar to or smaller than that of wild type (Fig. 2), and in such cases more latitude exists with respect to the determination of k_B and k_C (51). A reduced overshoot can result either from an inhibition of phosphoenzyme processing or from an enhanced Ca^{2+} binding transition, or a combination of both. Direct measurements of the rates of the partial reactions involved in phosphoenzyme and dephosphoenzyme processing are presented below.

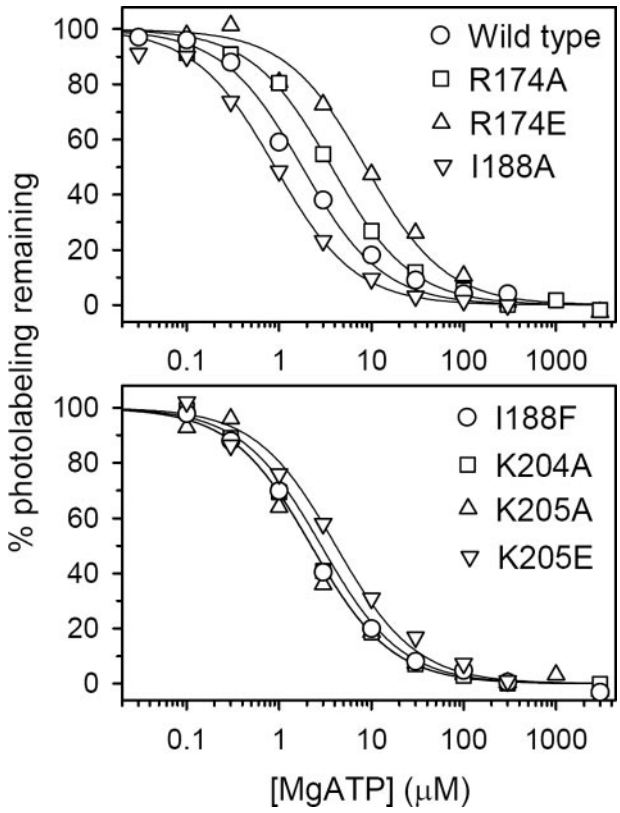

FIGURE 3. **Binding of MgATP determined by competition with [γ-^{32}P]TNP-8N_3-MgATP photolabeling.** Photolabeling of expressed wild type or mutants was performed in 25 mM EPPS/tetramethylammonium hydroxide (pH 8.5), 20% (v/v) glycerol, 0.5 mM EGTA, a [γ-^{32}P]TNP-8N_3-ATP concentration of 3× the $K_{0.5}$ for TNP-8N_3-MgATP (Table 2), the indicated concentrations of ATP, and 1 mM $MgCl_2$ in excess over the ATP concentration. The *lines* represent the best fits to the data of a hyperbolic function as described under "Experimental Procedures." Table 2 lists the K_D values derived from the data.

Affinity of E1 for MgATP—The nucleotide binding properties of wild type and mutants were examined in the absence of Ca^{2+} (to avoid ATP hydrolysis) and at pH 8.5 (to accumulate $E1$ even in the absence of Ca^{2+} (55)), by using the previously described and validated assay in which the ATPase is photolabeled with [γ-^{32}P]TNP-8N_3-MgATP (30, 46, 47, 49). The [γ-^{32}P]TNP-8N_3-MgATP dependence of the photolabeling and the competitive inhibition of the photolabeling with MgATP were studied, and results are shown in Fig. 3 and supplemental Fig. S2, with the derived affinity constants listed in Table 2. In accordance with the wild type-like phosphorylation rates obtained with the mutants at a subsaturating concentration of MgATP (Fig. 2), the effects of the mutations on nucleotide binding were moderate. Thus, the $K_{0.5}$ values for the binding of the photolabel and the K_D values for MgATP inhibition of the photolabeling generally deviated less than 2-fold from the values obtained with wild type (Table 2). Exceptions to this pattern, however, were R174E and I188A, the former displaying a significant and reproducible 4-fold reduced MgATP affinity relative to wild type, and the latter displaying 2–3-fold increased TNP-8N_3-MgATP and MgATP affinities, suggesting that under the conditions of the binding assay Arg^{174} and Ile^{188} may interact with the nucle-

TABLE 2

Nucleotide binding affinities determined at pH 8.5 and in the absence of Ca^{2+} by [γ-^{32}P]TNP-8N$_3$-MgATP photolabeling and MgATP inhibition thereof

	TNP-8N$_3$-MgATP,[a] $K_{0.5}$	MgATP,[b] K_D
	μM	μM
Wild type	0.79	0.51
R174A	0.58	0.93
R174E	0.63	2.17
I188A	0.33	0.23
I188F	0.54	0.56
K204A	0.85	0.56
K205A	0.44	0.71
K205E	1.26	1.03

[a] Affinity constants for [γ-^{32}P]TNP-8N$_3$-MgATP binding to Ca^{2+}-free enzyme at pH 8.5 derived from the analysis of the data presented in supplemental Fig. S2.
[b] Affinity constants for MgATP binding to Ca^{2+} free enzyme at pH 8.5 derived from the analysis of the data presented in Fig. 3.

otide to a slightly more significant extent than seen in the phosphorylation assay described above. The flexibility of the A-domain may be higher in the absence of Ca^{2+} than in its presence, thereby allowing the A-domain to "sample" *E*2 conformations, in which Arg^{174} comes close to and possibly interacts with the nucleotide (see under "Discussion"). Studies of the ADP dependence of ADP-induced dephosphorylation of phosphoenzyme formed from 5 μM [γ-^{32}P]MgATP also showed only moderate deviations of the mutants from wild type with respect to the $K_{0.5}$ for ADP, suggesting that the mutations interfere little with ADP binding to Ca_2E1P (supplemental Fig. S3).

Ca_2E1P to E2P Transition and Its Modulation by MgATP—Phosphorylation of Ca_2E1 from MgATP leads to formation of the Ca_2E1P phosphoenzyme, which subsequently undergoes a conformational transition to the Ca_2E2P state (56), followed by the release of the two Ca^{2+} ions to the lumenal side of the membrane and thus formation of Ca^{2+}-free *E*2P (*cf.* Scheme 1). The $Ca_2E1P \rightarrow E2P$ transition is a rate-limiting reaction step in the overall pump cycle under normal physiological conditions (57) and therefore an obvious target for regulation of activity. Indeed, acting in a nonphosphorylating modulatory mode, MgATP has a prominent activating effect on the rate of the conformational change of the phosphoenzyme (22–25, 30).

The time course of the forward processing of phosphoenzyme formed by phosphorylation of Ca^{2+}-saturated enzyme from 5 μM [γ-^{32}P]MgATP was measured by a chase of the accumulated phosphoenzyme with excess EGTA (to remove Ca^{2+} and thus terminate phosphorylation) and varying concentrations of nonradioactive MgATP. Under the phosphorylation conditions applied here (0 °C at pH 7 and high [K^+]), the steady-state phosphoenzyme accumulated prior to the initiation of the chase was almost exclusively ADP-sensitive Ca_2E1P for wild type as well as mutants (supplemental Fig. S3), demonstrating that the conformational transition of the phosphoenzyme (*i.e.* $Ca_2E1P \rightarrow E2P$) was indeed the rate-limiting step in phosphoenzyme processing. The dephosphorylation time courses obtained at selected MgATP concentrations are shown in supplemental Fig. S4, and the basic rate constants (*i.e.* those corresponding to absence of MgATP in excess of the amount used for phosphorylation) obtained by fitting of a monoexponential decay function to the data are listed in Table 1 (column labeled "$Ca_2E1P \rightarrow E2P$"). R174E and I188A displayed significant 8- and 3-fold reduced basic rates of $Ca_2E1P \rightarrow E2P$ relative

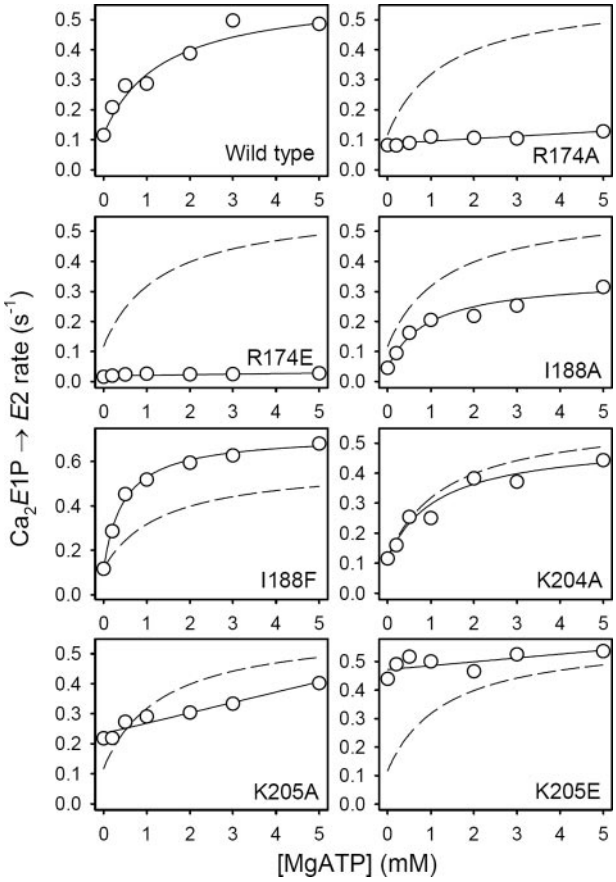

FIGURE 4. **MgATP dependence of the rate of forward processing of Ca_2E_1P phosphoenzyme.** The dephosphorylation rate constants derived from the data in supplemental Fig. S4 and from data obtained in a similar way at other MgATP concentrations in the chase medium are shown here as a function of the MgATP concentration. The *lines* represent the best fits to the data of the hyperbolic function described under "Experimental Procedures" (see Equation 1), the derived parameters being listed in Table 3 (column $Ca_2E_1P \rightarrow E_2P$, MgATP). The *broken lines* correspond to the wild type curve from the *top left panel*.

to wild type, whereas the rate of R174A was only mildly reduced, and the rates of I188F and K204A were wild type-like. K205A and K205E displayed 2- and 4-fold enhanced basic rates of $Ca_2E1P \rightarrow E2P$, respectively, in accordance with the large, steep phosphorylation overshoots seen with these two mutants in the phosphorylation time courses described above (Fig. 2).

The MgATP dependence of the rate of phosphoenzyme processing starting from Ca_2E1P (*i.e.* $Ca_2E1P \rightarrow E2P$) is shown in Fig. 4, and the affinity constants ($K_{0.5}$) and enhancement factors (k_{max}/k_0, *i.e.* the ratio between the maximum rate and the basic rate) for the MgATP-induced stimulation derived from fits of a hyperbolic function to the data are listed in Table 3 (columns labeled "$Ca_2E1P \rightarrow E2P$, MgATP"). For wild type, the analysis provided an MgATP affinity of 1.35 mM and an enhancement factor of 5.0, in good agreement with our previously published values of 1.44 mM and 4.7, respectively (30). K204A deviated only marginally from the wild type in these respects. MgATP enhanced the $Ca_2E1P \rightarrow E2P$ rates of I188A and I188F to an extent slightly higher than that of wild type (k_{max}/k_0 of 7.5 and 6.2, respectively) and with somewhat increased MgATP affinities (1.6- and 2.9-fold, respectively). In contrast, R174A and R174E displayed almost no MgATP-in-

TABLE 3
Affinity constants and enhancement factors for the modulation of partial reactions by nucleotide and PP_i

	$Ca_2E1P \rightarrow E2P$[a] MgATP		$E2P \rightarrow E2$[b] ATP		$E2P \rightarrow E2$[c] PP_i		$H_nE2 \rightarrow Ca_2E1$[d] MgATP	
	$K_{0.5}$	k_{max}/k_0	$K_{0.5}$	k_{max}/k_0	$K_{0.5}$	k_{max}/k_0	$K_{0.5}$	k_{max}/k_0
	mM		μM		mM		μM	
Wild type	1.35	5.0	34	2.4	3.0	4.7	37	34
R174A	NM[e]		258	4.9	1.7	3.5	29	17
R174E	NM		>500	>3	LA	>2	28	9
I188A	0.85	7.5	NM		1.5	2.4	37	27
I188F	0.46	6.2	77	4.6	2.2	6.0	~96[f]	>14
K204A	1.17	4.4	62	2.3	2.0	3.2	44	32
K205A	LA[g]	>1.7	33	0.32	NM		38	30
K205E	NM		107	0.26	NM		~95[f]	>14

[a] Affinity constants and enhancement factors for MgATP modulation of $Ca_2E1P \rightarrow E2P$ were derived from the analysis of the data presented in Fig. 4.
[b] Affinity constants and enhancement factors for ATP modulation of *E*2P dephosphorylation were derived from the analysis of the data presented in Fig. 5.
[c] Affinity constants and enhancement factors for PP_i modulation of *E*2P dephosphorylation were derived from the analysis of the data presented in Fig. 6.
[d] Affinity constants and enhancement factors for MgATP modulation of $H_nE2 \rightarrow Ca_2E2$ were derived from the analysis of the data presented in Fig. 7.
[e] NM, no significant modulation was observed over the concentration range of the substrate studied. This could in principle mean very low affinity or that binding occurs without being productive (*i.e.* $k_{max}/k_0 \sim 1$).
[f] For I188F and K205E, which display wild type-like basic rates (k_0) of $H_nE2 \rightarrow Ca_2E1$ (*cf.* Table 1), the $K_{0.5}$ value for the modulation by MgATP of $H_nE2 \rightarrow Ca_2E1$ was deduced under the assumption that the k_{max} is also wild type-like.
[g] LA means low affinity. Here, $k_{max} > k_0$, but the rate did not reach a constant level within the concentration range of substrate applied, thus excluding reliable evaluation of an affinity constant.

duced activation of phosphoenzyme processing throughout the MgATP concentration range studied, and accordingly, no MgATP affinity constant could be obtained for these two mutants. The ability of K205A and K205E to undergo MgATP-induced stimulation of phosphoenzyme processing was also notably impaired. Thus, K205A displayed only a 1.7-fold enhancement of phosphoenzyme processing over the MgATP concentration range applied, suggesting very low MgATP affinity (although a $K_{0.5}$ value could not be derived), and in K205E the affinity appeared even lower with almost no MgATP modulation throughout the nucleotide concentration range.

Dephosphorylation of E2P and Its Modulation by ATP—Like the $Ca_2E1P \rightarrow E2P$ conformational transition of the phosphoenzyme, the dephosphorylation of *E*2P is also a target for stimulatory modulation by nucleotide in a nonphosphorylating mode (22, 24, 26–28, 30). Contrary, however, to the nucleotide modulation of $Ca_2E1P \rightarrow E2P$, which is rather independent of whether Mg^{2+} is present or absent (30), the modulation of $E2P \rightarrow E2$ depends on metal-free ATP. High concentrations of Mg^{2+} eliminate the accelerating effect, because only metal-free ATP binds to *E*2P with reasonable affinity (in the 10–100 μM range) (24, 28–30).

To study the rate of *E*2P dephosphorylation, wild type and mutants were phosphorylated by $^{32}P_i$ in the reverse direction relative to the normal turnover cycle, under favorable conditions for *E*2P accumulation (saturating concentration of $^{32}P_i$ and Mg^{2+}, absence of Ca^{2+}, acidic pH, presence of dimethyl sulfoxide, and absence of K^+). Next, the phosphoenzyme decay was followed upon a chase of the accumulated phosphoenzyme with excess EDTA (to chelate Mg^{2+} and thus terminate phosphorylation) and varying concentrations of ATP. The time courses obtained with wild type and mutants at selected ATP concentrations are shown in supplemental Fig. S5, and the basic rate constants (*i.e.* those obtained in the absence of ATP) are listed in Table 1 (column labeled "$E2P \rightarrow E2$"). In the absence of ATP, R174E, K205A, and K205E displayed significantly reduced *E*2P stability relative to wild type (4.1-, 3.6-, and 7.9-fold increased basic rate constants, respectively), whereas the rate constants obtained with R174A, I188A, I188F, and K204A deviated less than 2-fold from that of wild type.

The ATP dependence of the rate of *E*2P dephosphorylation is shown in Fig. 5, and the ATP affinities and enhancement factors derived from fits of a hyperbolic function to the data are listed in Table 3 (columns labeled "$E2P \rightarrow E2$, ATP"). For wild type, the affinity of *E*2P for ATP was found to be 34 μM with an enhancement factor of 2.4, comparable with our previously published values of $K_{0.5}$ = 19 μM and k_{max}/k_0 = 2.9 (30). The parameters derived from the analysis of K204A deviated only marginally from those of wild type (1.8-fold reduced ATP affinity and wild type-like enhancement factor). In contrast, R174A and R174E displayed 7.6- and, at least, 15-fold reduced ATP affinities, respectively (note the different scales on the *abscissa* for R174A and R174E in Fig. 5), but with significant (more than 3-fold) activation of *E*2P dephosphorylation over the range of ATP concentrations applied, suggesting involvement of the Arg^{174} side chain in binding of the modulatory ATP to *E*2P. The dephosphorylation of I188A was not modulated by ATP throughout the concentration range studied. On the contrary, the *E*2P dephosphorylation of I188F was modulated quite efficiently (k_{max}/k_0 = 4.6) by ATP with an affinity only 2.2-fold lower than that of wild type, implying that a bulky, hydrophobic side chain at position 188 is a prerequisite for a functional modulatory ATP-binding site in *E*2P. Contrary to the wild type, the rates of *E*2P dephosphorylation of K205A and K205E showed a surprising inhibition by ATP, rather than stimulation. Thus, whereas the basic rate of K205A was 4-fold enhanced relative to wild type, the rate obtained in the presence of 1 mM ATP was, in fact, 2-fold lower than that of the wild type. Similarly, for K205E, the basic rate was 8-fold enhanced relative to the wild type, and the rate obtained in the presence of 1 mM ATP was wild type-like. Remarkably, the affinity for the *inhibition* by ATP of *E*2P dephosphorylation in K205A was 33 μM, *i.e.* identical to the affinity for the *stimulation* of *E*2P dephosphorylation by ATP in the wild type ($K_{0.5}$ = 34 μM). The $K_{0.5}$ of K205E was only 3-fold higher (*i.e.* lower affinity) than that of the wild type.

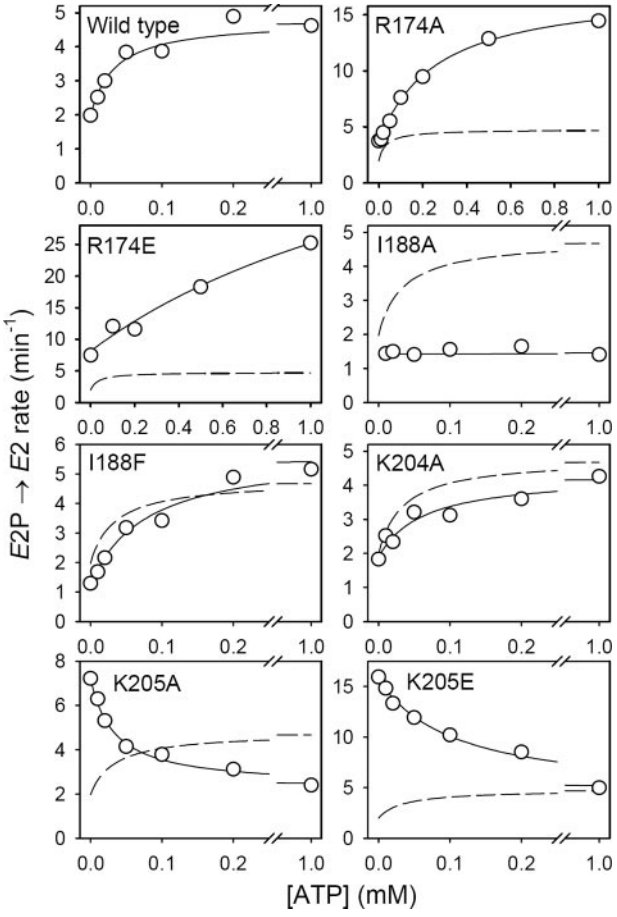

FIGURE 5. **ATP dependence of the rate of dephosphorylation of E_2P.** The dephosphorylation rate constants derived from the data in supplemental Fig. S5 and from data obtained in a similar way at other ATP concentrations in the chase medium are shown here as a function of the ATP concentration. Note the different scales on the *ordinate* in the different panels, reflecting the marked effects of some of the mutations on the dephosphorylation rate. Note also the different scales on the *abscissa* for R174A and R174E, reflecting the reduced ATP affinity of these two mutants. The *lines* represent the best fits of the hyperbolic function described under "Experimental Procedures" (see Equation 1), the derived parameters being listed in Table 3 (column $E_2P \rightarrow E_2$, ATP). The *broken lines* correspond to the wild type curve from the *top left panel*.

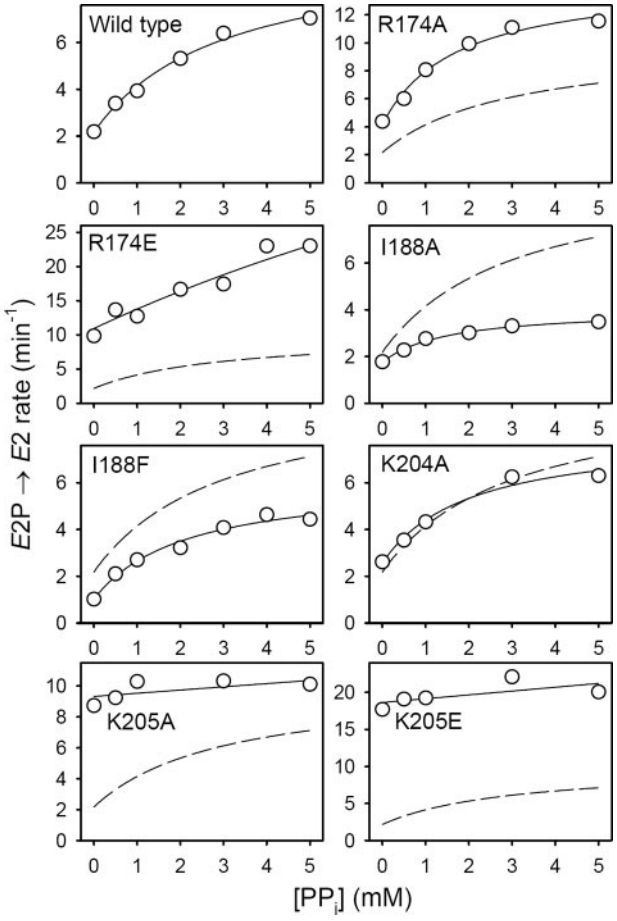

FIGURE 6. **PP_i dependence of the rate of dephosphorylation of E_2P.** The dephosphorylation rate constants derived from the data in supplemental Fig. S6 and from data obtained in a similar way at other PP_i concentrations in the chase medium are shown here as a function of the PP_i concentration. Note the different scales on the *ordinate* in the different panels. The *lines* represent the best fits of the hyperbolic function described under "Experimental Procedures" (see Equation 1), the derived parameters being listed in Table 3 (column $E_2P \rightarrow E_2$, PP_i). The *broken lines* correspond to the wild type curve from the *top left panel*.

Modulation of E2P Dephosphorylation by PP_i—Millimolar concentrations of PP_i (pyrophosphate) exert a stimulatory effect on the overall ATP turnover rate, resembling the low affinity effect of ATP/MgATP on ATPase activity (58). Furthermore, PP_i has been shown to competitively inhibit the binding of both ATP and the phosphate transition-state analogue vanadate to Ca^{2+}-deprived *E*2, in either case with an affinity around 1–2 mM (58–60), suggesting overlapping binding sites for PP_i, vanadate, and the modulatory nucleotide.

To study the ability of PP_i to modulate $E2P \rightarrow E2$, we measured the PP_i dependence of the rate of *E*2P dephosphorylation. The method was essentially the same as that described above for the ATP dependence of *E*2P dephosphorylation, except that ATP was replaced by PP_i. The results are shown in Fig. 6, with the time courses at selected PP_i concentrations depicted in supplemental Fig. S6, and the PP_i affinities and enhancement factors derived from fits of a hyperbolic function to the data listed in Table 3 (columns labeled "$E2P \rightarrow E2$, PP_i"). It is seen in Fig. 6 that the rate of *E*2P dephosphorylation of the wild type is accelerated by PP_i with an affinity constant of 3 mM and an enhancement factor of 4.7. K204A and R174A deviated only marginally from wild type with respect to affinities and enhancement factors. R174E displayed 2.3-fold higher rate at 5 mM PP_i than in its absence and a significantly reduced PP_i affinity (an affinity constant could not, however, be derived for R174E, because the dephosphorylation rate did not reach a steady level within the concentration range of PP_i applied). I188A and I188F both displayed affinities for PP_i at least as high as that of the wild type, although the enhancement factor of I188A was only 2.4 compared with 6.0 for I188F. The ability of I188A to undergo PP_i-induced stimulation of *E*2P dephosphorylation sharply contrasts its insensitivity to ATP modulation, suggesting that Ile^{188} contributes to ligation of the adenosine moiety of the modulatory ATP in *E*2P. Neither K205A nor K205E were able to undergo PP_i-induced stimulation of $E2P \rightarrow E2$, both mutants displaying a rather constant high *E*2P dephosphorylation rate throughout the PP_i concentration range studied.

$H_nE2 \rightarrow Ca_2E1$ Transition and Its Modulation by MgATP—The rate of the Ca^{2+} binding transition of the dephosphoenzyme (*i.e.* $H_nE2 \rightarrow Ca_2E1$, involving proton dissociation and

Ca^{2+} binding) was first examined in the absence of nucleotide. The wild type or mutant enzyme was pre-equilibrated in the absence of Ca^{2+} at pH 6 to accumulate the *E*2 state, followed by incubation with excess Ca^{2+} for varying time intervals and subsequent incubation with [γ-^{32}P]MgATP for 34 ms. This assay takes advantage of the fact that only the Ca_2E1 state can be phosphorylated by MgATP (61) and that the phosphorylation step is much faster than the preceding deprotonation and Ca^{2+} binding conformational changes for mutants as well as wild type (*cf.* Table 1). The amount of phosphoenzyme obtained for each time interval of Ca^{2+} incubation thus reflects the amount of Ca_2E1 present prior to the addition of [γ-^{32}P]MgATP. The time courses of $H_nE2 \rightarrow Ca_2E1$ obtained from such experiments are shown in supplemental Fig. S7*A*, and the rate constants derived from fits of a monoexponential function to the data are listed in Table 1 (column labeled "$H_nE2 \rightarrow Ca_2E1$"). Only R174E displayed a basic rate of $H_nE2 \rightarrow Ca_2E1$ deviating more than 2-fold from that of the wild type (2.7-fold enhanced rate).

Next, we studied the ability of MgATP to accelerate $H_nE2 \rightarrow Ca_2E1$. The enzyme was again pre-equilibrated in the absence of Ca^{2+} at pH 6 to accumulate H_nE2, and the $H_nE2 \rightarrow Ca_2E1 \rightarrow Ca_2E1P$ reaction sequence was then followed by simultaneous addition of excess Ca^{2+} and varying concentrations of [γ-^{32}P]MgATP, with subsequent acid quenching at varying time intervals. The resulting time courses obtained at selected MgATP concentrations are shown in supplemental Fig. S7*B*. As noted above, the Ca^{2+} binding transition is considerably slower than the subsequent phosphorylation step at pH 6 for wild type as well as mutants (*cf.* Table 1), and the observed time course of phosphoenzyme formation thus reflects the rate of $H_nE2 \rightarrow Ca_2E1$. In Fig. 7, the measured rate constants are shown as a function of the MgATP concentration, and Table 3 lists the MgATP affinity constants ($K_{0.5}$) and enhancement factors (k_{max}/k_0) derived from fits of a hyperbolic function to the data (columns labeled "$H_nE2 \rightarrow Ca_2E1$, MgATP"). For the wild type, the MgATP affinity determined was 37 μM with an enhancement factor of 34, in good agreement with our previously published values (30). The parameters derived from the analysis of I188A, K204A, and K205A were almost identical to those obtained with the wild type. R174A and R174E displayed wild type-like MgATP affinities, but 2.0- and 3.8-fold reduced enhancement factors, respectively, possibly related to their respective 2- and 3-fold enhanced basic rates of $H_nE2 \rightarrow Ca_2E1$ (Table 1). I188F and K205E both displayed reduced MgATP affinity. Thus, in both mutants the basic rate of $H_nE2 \rightarrow Ca_2E1$ was almost identical to that of wild type, whereas the rates measured at MgATP concentrations in the 5–50 μM range were significantly reduced. The low MgATP affinities of I188F and K205E excluded an accurate determination of the affinity constants for these two mutants. However, assuming that the k_{max} value of I188F and K205E is wild type-like (*i.e.* corresponding to wild type-like enhancement factors, because of the fact that the k_0 is wild type-like for both mutants), their $K_{0.5}$ for MgATP would be ~100 μM (Table 3), *i.e.* 3-fold reduced MgATP affinity relative to wild type.

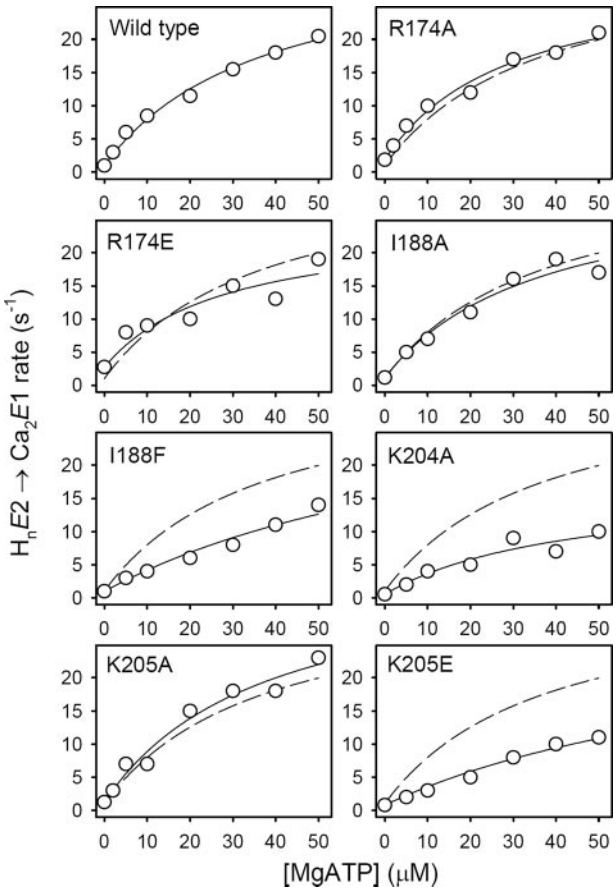

FIGURE 7. **MgATP dependence of the rate of the Ca^{2+} binding transition.** The $H_nE_2 \rightarrow Ca_2E_1$ rate constants derived from the data in supplemental Fig. S7 and from data obtained in a similar way at other MgATP concentrations in the phosphorylation medium are shown here as a function of the MgATP concentration. The *lines* represent the best fits to the data of the hyperbolic function described under "Experimental Procedures" (see Equation 1), the derived parameters being listed in Table 3 (column $H_nE_2 \rightarrow Ca_2E_1$, MgATP). The *broken lines* correspond to the wild type curve from the *top left panel*.

DISCUSSION

Here we have investigated the functional consequences of mutations to Arg^{174}, Ile^{188}, Lys^{204}, and Lys^{205} in the A-domain of the Ca^{2+}-ATPase, and the results demonstrate that the A-domain is an important player in the function of ATP as nonphosphorylating modulator of the partial reaction steps, with Arg^{174}, Ile^{188}, and Lys^{205} all being critically involved in the stimulation of phosphoenzyme processing by nucleotide, although in different ways.

The crystal structures of the Ca^{2+}-ATPase provide useful (although not necessarily perfect) models of the various conformational states of the enzyme cycle, and for the present purpose of discussing the mutational effects on nucleotide interaction, it is helpful to consider the arrangement of the nucleotide binding region in the crystal structures in some detail, in particular the contribution of the A-domain (Fig. 8). During the transport cycle, the A-domain undergoes quite dramatic movements relative to the N- and P-domains. The intermediates Ca_2E1·ATP and Ca_2E1P·ADP are represented by the crystal structures of Ca_2E1·AMPPCP (5, 7) and Ca_2E1P·AMPPN (11), respectively, the γ-phosphate of AMPPNP being transferred to Asp^{351} in the latter. In these structures, residues in the N- and P-domains

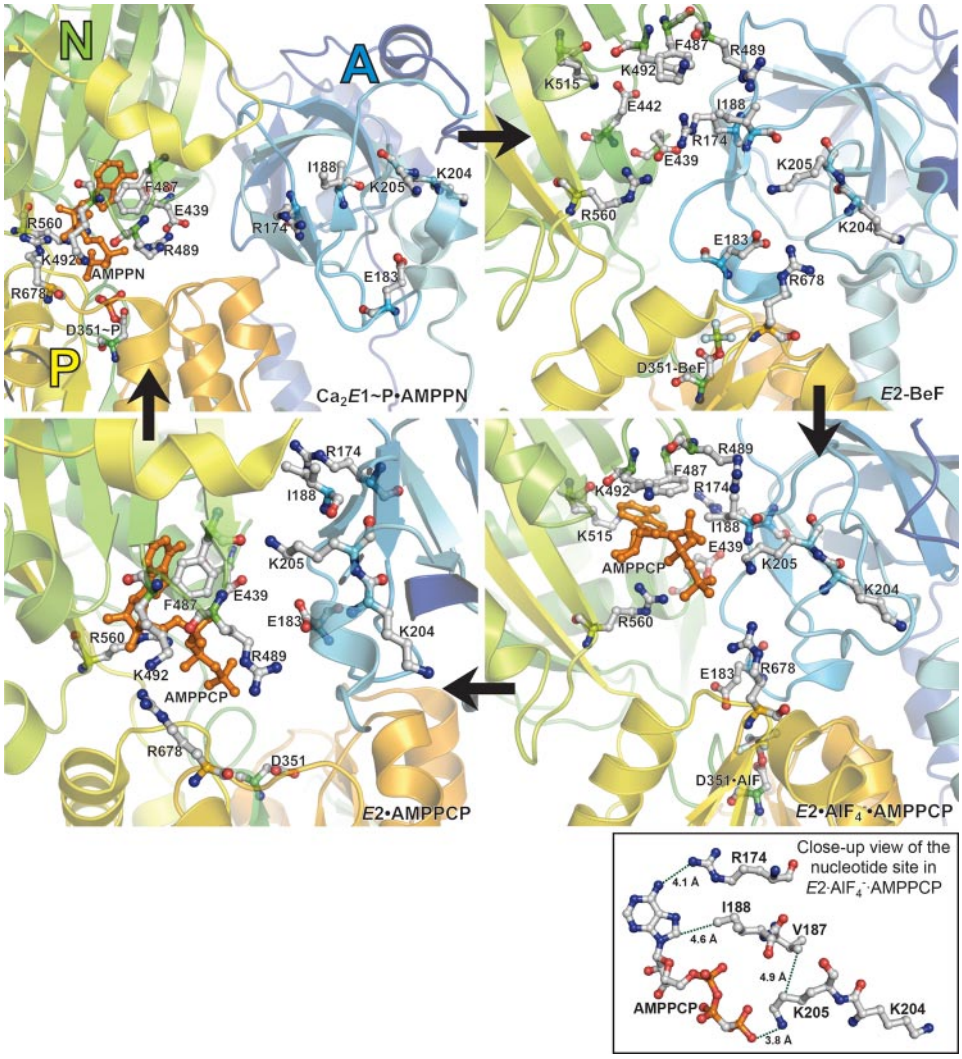

FIGURE 8. **Structural arrangement of Arg^{174}, Ile^{188}, Lys^{204}, and Lys^{205} in relation to the nucleotide-binding site in Ca^{2+}-ATPase crystallized in the Ca$_2$*E*1P·ADP state (*Ca$_2$E1P·AMPPN*), the *E*2P state (*E2·BeF$_3^-$*), the *E*2·P·ATP transition state (*E2·AlF$_4^-$·AMPPCP*), and the *E*2·ATP state (*E2·AMPPCP*).** The respective Protein Data Bank accession codes corresponding to the structures shown are 3BA6 (11), 3B9B (11), 3B9R (11), and 2C88 (9). Amino acid side chains are shown for residues discussed in the text. Carbon and aluminum atoms are shown in *gray*, beryllium in *green*, nitrogen in *blue*, oxygen in *red*, fluoride in *cyan*, and phosphorus and nucleotide in *orange* (except in the *boxed* close-up view of the nucleotide site in *E*2·AlF$_4^-$·AMPPCP, in which the nucleotide is shown with carbon atoms in *gray*, oxygen in *red*, nitrogen in *blue*, and phosphorus in *orange*). *Arrows* indicate the direction of the enzyme cycle. The phosphorylation, nucleotide binding, and actuator domains are indicated by "*P*," "*N*," and "*A*," respectively.

form a tight complex with the nucleotide at the catalytic site, whereas the A-domain does not contribute to nucleotide binding (Fig. 8, *upper left panel*), in good agreement with our data showing that for all the mutants analyzed functionally here the rate of phosphorylation of Ca$_2$*E*1 from a subsaturating concentration of MgATP was indistinguishable from that of the wild type. Following Ca$_2$*E*1P formation, an ~90° clockwise rotation (viewed from the cytoplasm) of the A-domain in a plane roughly parallel to the membrane allows for the insertion of the conserved ^{181}TGES phosphatase motif (38) of the A-domain into a cleft formed between the P- and N-domains, leading to the *E*2P ground state (represented by the *E*2·BeF$_3^-$ crystal structure (10, 11) shown in Fig. 8, *upper right panel*). The *E*2·BeF$_3^-$ structure was obtained in the absence of nucleotide; however, docking of ADP or ATP into the structure on the basis of a structural alignment of the N-domain provided a "snug fit" with Arg^{174} binding the nucleotide (11). During the Ca$_2$*E*1P → *E*2P transition ADP dissociates from the catalytic site (whether ADP actually dissociates before (10) or after (11, 62) the A-domain rotation is not clear). Moreover, the A-domain rotation leads to opening of the Ca^{2+} sites toward the lumen and release of the Ca^{2+} ions (56). In *E*2P, a subsequent further ~25° rotation of the A-domain brings Glu^{183} in the ^{181}TGES motif in position for binding the water molecule attacking the aspartyl phosphate (38), thus resulting in initiation of the hydrolysis by formation of the *E*2·P transition state (represented by the *E*2·AlF$_4^-$·AMPPCP crystal structure (11) shown in Fig. 8, *lower right panels*). In the latter structure, the side chains of Arg^{174}, Ile^{188}, and Lys^{205} are closely associated with the bound nucleotide in good agreement with our findings of mutational effects on ATP modulation of *E*2P dephosphorylation. The liberation of the phosphoryl group from the catalytic site seems to be accompanied by the N-domain swinging back down upon the P-domain, the ^{181}TGES motif in the A-domain leaving the catalytic site and Arg^{174}, Ile^{188}, and Lys^{205} retreating from their association with the nucleotide (*cf.* Fig. 8, *lower left panel*, showing the *E*2·AMPPCP crystal structure (9), representing *E*2·ATP). Completion of the cycle is associated with a reversal of the A-domain rotation during the Ca^{2+}-binding H$_n$*E*2 → Ca$_2$*E*1 transition (4). The role of the modulatory nucleotide in connection with H$_n$*E*2 → Ca$_2$*E*1 is probably to help release the A-domain from the P-domain by interfering with inter-domain bonds (30). Our results indicating that alanine mutations to Arg^{174}, Ile^{188}, Lys^{205}, and Lys^{205} do not disturb the modulation of the H$_n$*E*2 → Ca$_2$*E*1 transition by nucleotide are in good accordance with the *E*2·AMPPCP structure, where these A-domain residues neither bind to the nucleotide nor to the P-domain (Fig. 8, *lower left panel*).

Role of Arg^{174}—The quite moderate effects of the R174A mutation on the basic rates of Ca$_2$*E*1P → *E*2P, *E*2P → *E*2, and H$_n$*E*2 → Ca$_2$*E*1 suggest that the Arg^{174} side chain is of minor mechanistic importance for the progression of the conformational transitions of the enzyme cycle in the absence of modulation by nonphosphorylating nucleotide, although the

significant slowing of phosphoenzyme processing in R174E indicates that Arg^{174} does approach other parts of the enzyme during the A-domain transitions. In the $E2{\cdot}BeF_3^-$ structure ($E2P$ ground state analog) the side chain of Arg^{174} is indeed only 4.2 Å from that of Glu^{439} of the N-domain (*upper right panel* in Fig. 8).

Both R174A and R174E were severely affected with respect to modulation by MgATP of the $Ca_2E1P \rightarrow E2P$ transition (Fig. 4). Moreover, both R174A and R174E displayed markedly reduced affinity for ATP modulation of $E2P$ dephosphorylation (Fig. 5). In contrast, the ability to undergo PP_i-induced stimulation of $E2P$ dephosphorylation was rather unaffected by the R174A mutation and even occurred to a significant extent in R174E, although the affinity for PP_i was significantly reduced in R174E (Fig. 6), showing that the PP_i senses the negative charge of the glutamate side chain. These observations support the hypothesis that the role of Arg^{174} in nucleotide modulation of $Ca_2E1P \rightarrow E2P$ and $E2P$ dephosphorylation relates to direct interactions with the nucleotide. Because PP_i may be considered representative of the phosphate moiety of ATP, it appears that, at least in connection with the modulation of $E2P$ dephosphorylation, it is the adenosine part of the nucleotide that interacts with Arg^{174}, thereby providing a functional correlate of the close proximity of Arg^{174} to the adenine ring seen in the $E2{\cdot}AlF_4^-{\cdot}$AMPPCP structure ($E2{\cdot}P$ transition state analog, Fig. 8, *lower right panels*).

Role of Ile^{188}—The reduced basic rate of $Ca_2E1P \rightarrow E2P$ in $I188A$ suggests that Ile^{188}, like Arg^{174}, may interact with other parts of the enzyme during the $Ca_2E1P \rightarrow E2P$ transition. MgATP modulation of $Ca_2E1P \rightarrow E2P$ in I188A and I188F occurred with affinities and enhancement factors at least as high as that of wild type, indicating that Ile^{188} is not crucial to the interaction with the nucleotide modulating $Ca_2E1P \rightarrow E2P$. In contrast, the stimulation by ATP of $E2P$ dephosphorylation was completely abolished in I188A. I188F, on the other hand, displayed only a moderate 2-fold reduction of affinity for the modulation by ATP of $E2P$ dephosphorylation, showing that a bulky hydrophobic side chain at position 188 is a prerequisite for ATP modulation of this reaction step. Contrasting the conspicuous effect of the I188A mutation on the modulation by ATP, the affinity of I188A for the PP_i-induced modulation of $E2P$ dephosphorylation was at least as high as that of the wild type. Hence, Ile^{188} may contribute directly to the binding of the adenosine moiety of the modulatory nucleotide in the $E2{\cdot}P$ transition state. In the $E2{\cdot}AlF_4^-{\cdot}$AMPPCP crystal structure Ile^{188} is indeed closer to the adenine ring than to other parts of the nucleotide (*lower right panels* in Fig. 8).

Role of Lys^{204}—The effect of the Lys^{204} mutations on the protein expression level in COS-1 cells suggests that Lys^{204} is a critical residue for post-transcriptional or post-translational events. Because Lys^{204} is mostly buried within the A-domain (Fig. 8), it may be of importance for the folding of the A-domain. The functional studies carried out with K204A generally showed wild type-like behavior, in particular with respect to the modulation by nucleotide of the partial reactions, in accordance with the Lys^{204} side chain facing in the opposite direction relative to Arg^{174}, Ile^{188}, and Lys^{205}, *i.e.* away from the nucleotide in the $E2$ forms.

Role of Lys^{205}—Contrary to Lys^{204}, the Lys^{205} side chain is unmistakably critical for the phosphoenzyme processing steps, as evidenced by the enhanced basic rates of $Ca_2E1P \rightarrow E2P$ and $E2P$ dephosphorylation in K205A and K205E (Table 1). Even more intriguing are the effects of the mutations to Lys^{205} on the modulation by MgATP/ATP of phosphoenzyme processing. Thus, K205A displayed rather low affinity for modulation by MgATP of $Ca_2E1P \rightarrow E2P$, and in K205E there was almost no MgATP modulation of $Ca_2E1P \rightarrow E2P$ (Fig. 4). Remarkably, rather than stimulating the dephosphorylation of $E2P$, as seen for wild type, ATP inhibited this partial reaction step in K205A and K205E (Fig. 5). The affinity of K205A for the *inhibition* by ATP of $E2P$ dephosphorylation was indistinguishable from the affinity of the wild type for the *stimulation* by ATP of $E2P$ dephosphorylation (Table 3), and the affinity of K205E was only 3-fold lower, showing that Lys^{205} is not very critical for the binding of the nucleotide modulating $E2P$ dephosphorylation, even though it is only 3.8 Å from the terminal phosphate of AMPPCP in the $E2{\cdot}AlF_4^-{\cdot}$AMPPCP structure and may interact through salt bridge formation (*lower right panels* in Fig. 8). Such interaction could, of course, require breakage of other bond(s) to the nucleotide, thereby explaining the unaltered affinity upon alanine substitution of Lys^{205}. Hence, the importance of Lys^{205} in connection with $E2P$ dephosphorylation may lie mostly in the mechanistic aspects, like transmittance of the effect of binding of ATP to the A-domain (see below), and not so much in contributing to the affinity for the nucleotide. The finding that in K205A and K205E the $E2P$ dephosphorylation was not stimulated by PP_i either is consistent with a mechanistic role of the interaction of Lys^{205} with the phosphate group, and it could mean that Lys^{205} is absolutely essential to PP_i binding.

Sites and Possible Mechanisms of the Modulatory Actions of Nucleotide on the Phosphoenzyme Processing Steps—It has been a controversial issue whether the ATP modulation of the Ca^{2+}-ATPase reaction cycle represents binding to a site (or sites) separate from the catalytic site (35, 36), and whether more than one ATP molecule might bind simultaneously on each Ca^{2+}-ATPase polypeptide chain (28, 33, 34). Our previous finding that the residues Phe^{487}, Arg^{560}, and Arg^{678} contributing to the binding of the phosphorylating ATP at the catalytic site are also critical for the stimulation by ATP of $E2P$ dephosphorylation clearly indicated some degree of overlap between the catalytic site and the modulatory nucleotide site on $E2P$ (or the $E2{\cdot}P$ transition state), but on the other hand these residues did not seem to contribute to binding of the MgATP molecule that modulates $Ca_2E1P \rightarrow E2P$ (30). The present findings with the Ile^{188} mutants likewise indicate that Ile^{188} is required for the binding of the ATP molecule modulating $E2P$ dephosphorylation, whereas Ile^{188} is not important for MgATP modulation of $Ca_2E1P \rightarrow E2P$, again suggesting that two different modulatory sites could be involved. Our data for Arg^{174} show, however, that this residue is critical to nucleotide modulation of either of these phosphoenzyme processing steps, thereby indicating a significant overlap between the two nucleotide sites involved with Arg^{174} contributing to both. Lys^{205} also seems to be involved in nucleotide modulation of $Ca_2E1P \rightarrow E2P$ as well as $E2P$ dephosphorylation, being a rather critical determinant of

TABLE 4
Conclusions regarding the functional roles of the amino acid residues studied

Residue	Partial reaction			
	$Ca_2E1 \rightarrow Ca_2E1P$	$Ca_2E1P \rightarrow E2P$	$E2P \rightarrow E2$	$H_nE2 \rightarrow Ca_2E1$
Arg^{174}	No prominent role	Contribution to binding of modulatory MgATP	Contribution to binding of the adenosine moiety of modulatory ATP	No prominent role
Ile^{188}	No prominent role	Critical for basic rate (reduced in alanine mutant) but not for modulation by MgATP	Contribution to binding of the adenosine moiety of modulatory ATP	No prominent role
Lys^{204}	No prominent role	No prominent role	No prominent role	No prominent role
Lys^{205}	No prominent role	Critical for basic rate (enhanced in mutants); contribution to binding of modulatory MgATP	Critical for basic rate (enhanced in mutants); critical for the modulatory effect of ATP binding (transmitted through phosphate moiety) with anomalous inhibition seen in mutants	No prominent role

the affinity for the MgATP modulating $Ca_2E1P \rightarrow E2P$ and playing a more mechanistic role in connection with the ATP modulation of *E*2P dephosphorylation. Both roles may be exerted through direct interaction with the nucleotide. Accordingly, none of the crystal structures published so far contains more than one nucleotide per Ca^{2+}-ATPase polypeptide chain, and in all cases the nucleotide is found in the same region of the protein. Taken together the data thus support a variable site model (37), in which the site is reconfigured from slightly different portions of the P-, N-, and A-domains in each of the conformational states occurring during the transport cycle. The modulatory nucleotide probably binds and dissociates several times in each major intermediate.

Although Arg^{174} and Lys^{205} are outside the possible range of interactions with nucleotide in the Ca_2E1P state, we nevertheless found that both residues are critical for the nucleotide modulation of $Ca_2E1P \rightarrow E2P$, implying that the modulation does not involve a destabilization of Ca_2E1P, but rather a stabilization of one or more of the subsequent *E*2-type intermediates where the A-domain has undertaken its ~90° rotation, bringing Arg^{174} and Lys^{205} into contact with the nucleotide. Stabilization of Ca_2E2P (a proposed intermediate state between Ca_2E1P and *E*2P (56)) relative to Ca_2E1P would indeed cause slowing of the back-reaction $Ca_2E2P \rightarrow Ca_2E1P$ and thus increase the net rate of the forward transition from Ca_2E1P to *E*2P. It seems likely that ATP/MgATP bound in exchange for the leaving ADP may assist in stabilizing Ca_2E2P relative to Ca_2E1P by bridging the interactions of the A-domain with the P- and N-domains. It emerges from our discussion that Arg^{174} and Lys^{205} would interact with the modulatory nucleotide in Ca_2E2P as well as in the *E*2·P transition state in the *E*2P dephosphorylation reaction, whereas Ile^{188} seems to interact with the nucleotide only in the *E*2·P transition state.

In the *E*2·P transition state the modulatory ATP may help to position the TGES motif of the A-domain in the optimal position for catalyzing hydrolysis of the aspartyl-phosphoryl bond. This leads us into an attempt to explain the compelling reversed mode of ATP modulation and the enhanced basic rate of *E*2P dephosphorylation found with K205A and K205E. In the $E2{\cdot}AlF_4^-{\cdot}$AMPPCP structure analog of the *E*2·P transition state, Lys^{205} is rather close to the side chain of Val^{187} and the backbone carbonyl group of Ile^{188}, both being part of the loop containing the TGES motif (see *close-up view* in Fig. 8). Hence, interference with Lys^{205}, either by nucleotide binding (probably fixing the lysine side chain) or by mutation, likely shifts the critical TGES loop, thus altering the rate of catalysis. Such effects would not be additive, because replacement of the Lys^{205} side chain prevents ATP from influencing the position of the TGES loop through this residue. Furthermore, if the nucleotide binds in a slightly different way in the mutant than in the wild type, because the Lys^{205} side chain has been replaced, then the positioning of the TGES loop for catalysis might even be disturbed rather than optimized by the nucleotide, thus explaining the nucleotide-induced inhibition of dephosphorylation in the Lys^{205} mutants.

The inhibition in the mutant Ca^{2+}-ATPases brings to mind the situation in the wild type Na^+,K^+-ATPase, for which it is well documented (31, 32) that *E*2P dephosphorylation is inhibited by nucleotide, and it also demonstrates that the opposite behaviors of the wild type Ca^{2+}- and Na^+,K^+-ATPases in response to ATP may be caused by rather subtle differences between these enzymes. A survey of the available P-type ATPase amino acid sequences and crystal structures (see supplemental Fig. S8 and associated table) clearly indicates a high conservation of positively charged residues corresponding to Arg^{174} and Lys^{205} among both the type IIA (SERCA) Ca^{2+}-ATPases and the type IIC (Na^+,K^+- and H^+,K^+-) ATPases, thus illustrating that their different responses to ATP is because of differences elsewhere; perhaps the presence of a polar serine or threonine in the Na^+,K^+-ATPase at the position corresponding to Ile^{188} in the Ca^{2+}-ATPase slightly changes the position of the modulatory ATP molecule and thereby its mode of interaction.

Conclusion—The A-domain is critically involved in the modulatory effects of MgATP/ATP on the rates of $Ca_2E1P \rightarrow E2P$ and *E*2P dephosphorylation. Arg^{174} is an important residue for binding of the modulatory nucleotide in both of these phosphoenzyme processing steps, whereas Ile^{188} interacts only with the ATP that modulates *E*2P dephosphorylation. Lys^{205} seems to be involved differentially in nucleotide modulation of $Ca_2E1P \rightarrow E2P$ and *E*2P dephosphorylation (Table 4).

Acknowledgments—We thank Lene Jacobsen and Karin Kracht (Aarhus University, Denmark) for expert technical assistance. Drs. Poul Nissen and Claus Olesen (Aarhus University, Denmark) are thanked for providing information about crystal structures prior to publication.

REFERENCES

1. Hasselbach, W., and Makinose, M. (1961) *Biochem. Z.* **333,** 518–528
2. Axelsen, K. B., and Palmgren, M. G. (1998) *J. Mol. Evol.* **46,** 84–101
3. Toyoshima, C., Nakasako, M., Nomura, H., and Ogawa, H. (2000) *Nature* **405,** 647–655
4. Toyoshima, C., and Nomura, H. (2002) *Nature* **418,** 605–611
5. Sørensen, T. L., Møller, J. V., and Nissen, P. (2004) *Science* **304,** 1672–1675
6. Olesen, C., Sørensen, T. L., Nielsen, R. C., Møller, J. V., and Nissen, P. (2004) *Science* **306,** 2251–2255
7. Toyoshima, C., and Mizutani, T. (2004) *Nature* **430,** 529–535
8. Toyoshima, C., Nomura, H., and Tsuda, T. (2004) *Nature* **432,** 361–368
9. Jensen, A. M., Sørensen, T. L., Olesen, C., Møller, J. V., and Nissen, P. (2006) *EMBO J.* **25,** 2305–2314
10. Toyoshima, C., Norimatsu, Y., Iwasawa, S., Tsuda, T., and Ogawa, H. (2007) *Proc. Natl. Acad. Sci. U. S. A.* **104,** 19831–19836
11. Olesen, C., Picard, M., Winther, A. M., Gyrup, C., Morth, J. P., Oxvig, C., Møller, J. V., and Nissen, P. (2007) *Nature* **450,** 1036–1042
12. Danko, S., Yamasaki, K., Daiho, T., and Suzuki, H. (2004) *J. Biol. Chem.* **279,** 14991–14998
13. Morth, J. P., Pedersen, B. P., Toustrup-Jensen, M. S., Sørensen, T. L., Petersen, J., Andersen, J. P., Vilsen, B., and Nissen, P. (2007) *Nature* **450,** 1043–1049
14. Pedersen, B. P., Buch-Pedersen, M. J., Morth, J. P., Palmgren, M. G., and Nissen, P. (2007) *Nature* **450,** 1111–1114
15. Shigekawa, M., and Dougherty, J. P. (1978) *J. Biol. Chem.* **253,** 1458–1464
16. de Meis, L., and Vianna, A. L. (1979) *Annu. Rev. Biochem.* **48,** 275–292
17. Scofano, H. M., Vieyra, A., and de Meis, L. (1979) *J. Biol. Chem.* **254,** 10227–10231
18. Wakabayashi, S., and Shigekawa, M. (1990) *Biochemistry* **29,** 7309–7318
19. Karlish, S. J., and Yates, D. W. (1978) *Biochim. Biophys. Acta* **527,** 115–130
20. Clarke, R. J., Apell, H. J., and Kong, B. Y. (2007) *Biochemistry* **46,** 7034–7044
21. Reenstra, W. W., Crothers, J., Jr., and Forte, J. G. (2007) *Biochemistry* **46,** 10145–10152
22. McIntosh, D. B., and Boyer, P. D. (1983) *Biochemistry* **22,** 2867–2875
23. Wakabayashi, S., Ogurusu, T., and Shigekawa, M. (1986) *J. Biol. Chem.* **261,** 9762–9769
24. Champeil, P., and Guillain, F. (1986) *Biochemistry* **25,** 7623–7633
25. Bodley, A. L., and Jencks, W. P. (1987) *J. Biol. Chem.* **262,** 13997–14004
26. Shigekawa, M., and Dougherty, J. P. (1978) *J. Biol. Chem.* **253,** 1451–1457
27. Ariki, M., and Boyer, P. D. (1980) *Biochemistry* **19,** 2001–2004
28. Champeil, P., Riollet, S., Orlowski, S., Guillain, F., Seebregts, C. J., and McIntosh, D. B. (1988) *J. Biol. Chem.* **263,** 12288–12294
29. Andersen, J. P., and Møller, J. V. (1985) *Biochim. Biophys. Acta* **815,** 9–15
30. Clausen, J. D., McIntosh, D. B., Anthonisen, A. N., Woolley, D. G., Vilsen, B., and Andersen, J. P. (2007) *J. Biol. Chem.* **282,** 20686–20697
31. Askari, A., and Huang, W. (1982) *Biochem. Biophys. Res. Commun.* **104,** 1447–1453
32. Mahmmoud, Y. A. (2008) *Proc. Natl. Acad. Sci. U. S. A.* **105,** 1757–1761
33. Cable, M. B., Feher, J. J., and Briggs, F. N. (1985) *Biochemistry* **24,** 5612–5619
34. Bishop, J. E., Al Shawi, M. K., and Inesi, G. (1987) *J. Biol. Chem.* **262,** 4658–4663
35. Coll, R. J., and Murphy, A. J. (1991) *Biochemistry* **30,** 1456–1461
36. Suzuki, H., Kubota, T., Kubo, K., and Kanazawa, T. (1990) *Biochemistry* **29,** 7040–7045
37. Clausen, J. D., McIntosh, D. B., Vilsen, B., Woolley, D. G., and Andersen, J. P. (2003) *J. Biol. Chem.* **278,** 20245–20258
38. Clausen, J. D., Vilsen, B., McIntosh, D. B., Einholm, A. P., and Andersen, J. P. (2004) *Proc. Natl. Acad. Sci. U. S. A.* **101,** 2776–2781
39. Kaufman, R. J., Davies, M. V., Pathak, V. K., and Hershey, J. W. (1989) *Mol. Cell. Biol.* **9,** 946–958
40. Maruyama, K., and MacLennan, D. H. (1988) *Proc. Natl. Acad. Sci. U. S. A.* **85,** 3314–3318
41. Vilsen, B., Andersen, J. P., and MacLennan, D. H. (1991) *J. Biol. Chem.* **266,** 16157–16164
42. Baginski, E. S., Foa, P. P., and Zak, B. (1967) *Clin. Chem.* **13,** 326–332
43. Sørensen, T., Vilsen, B., and Andersen, J. P. (1997) *J. Biol. Chem.* **272,** 30244–30253
44. Vilsen, B., Andersen, J. P., Clarke, D. M., and MacLennan, D. H. (1989) *J. Biol. Chem.* **264,** 21024–21030
45. Sørensen, T. L., Dupont, Y., Vilsen, B., and Andersen, J. P. (2000) *J. Biol. Chem.* **275,** 5400–5408
46. McIntosh, D. B., Woolley, D. G., Vilsen, B., and Andersen, J. P. (1996) *J. Biol. Chem.* **271,** 25778–25789
47. McIntosh, D. B., Woolley, D. G., MacLennan, D. H., Vilsen, B., and Andersen, J. P. (1999) *J. Biol. Chem.* **274,** 25227–25236
48. Clausen, J. D., McIntosh, D. B., Woolley, D. G., and Andersen, J. P. (2001) *J. Biol. Chem.* **276,** 35741–35750
49. McIntosh, D. B., Clausen, J. D., Woolley, D. G., MacLennan, D. H., Vilsen, B., and Andersen, J. P. (2004) *J. Biol. Chem.* **279,** 32515–32523
50. Clausen, J. D., McIntosh, D. B., Woolley, D. G., Anthonisen, A. N., Vilsen, B., and Andersen, J. P. (2006) *J. Biol. Chem.* **281,** 9471–9481
51. Clausen, J. D., and Andersen, J. P. (2004) *J. Biol. Chem.* **279,** 54426–54437
52. Inesi, G., Ma, H., Lewis, D., and Xu, C. (2004) *J. Biol. Chem.* **279,** 31629–31637
53. Lacapere, J. J., Bennett, N., Dupont, Y., and Guillain, F. (1990) *J. Biol. Chem.* **265,** 348–353
54. Lacapere, J. J., and Guillain, F. (1993) *Eur. J. Biochem.* **211,** 117–126
55. Forge, V., Mintz, E., and Guillain, F. (1993) *J. Biol. Chem.* **268,** 10961–10968
56. Daiho, T., Yamasaki, K., Danko, S., and Suzuki, H. (2007) *J. Biol. Chem.* **282,** 34429–34447
57. Champeil, P., le Maire, M., Andersen, J. P., Guillain, F., Gingold, M., Lund, S., and Møller, J. V. (1986) *J. Biol. Chem.* **261,** 16372–16384
58. Dupont, Y. (1977) *Eur. J. Biochem.* **72,** 185–190
59. Pick, U. (1982) *J. Biol. Chem.* **257,** 6111–6119
60. Arav, R., Aderem, A. A., and Berman, M. C. (1983) *J. Biol. Chem.* **258,** 10433–10438
61. Petithory, J. R., and Jencks, W. P. (1988) *Biochemistry* **27,** 5553–5564
62. McIntosh, D. B., Montigny, C., and Champeil, P. (2008) *Biochemistry* **47,** 6386–6393

Critical Interaction of Actuator Domain Residues Arginine 174, Isoleucine 188, and Lysine 205 with Modulatory Nucleotide in Sarcoplasmic Reticulum Ca^{2+}-ATPase

Johannes D. Clausen, David B. McIntosh, David G. Woolley and Jens Peter Andersen

J. Biol. Chem. 2008, 283:35703-35714.
doi: 10.1074/jbc.M806795200 originally published online October 17, 2008